RSC Advances

ROYAL SOCIETY OF CHEMISTRY

www.rsc.org/advances

TOC figure

Graphene/ZrO_2 composite aerogels with large BET area have been synthesized by a sol-gel method together with supercritical fluid drying process.

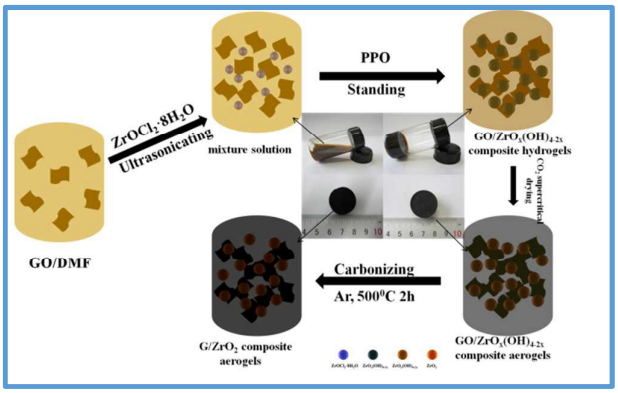

Cite this: DOI: 10.1039/c0xx00000x

www.rsc.org/xxxxxx

ARTICLE

Synthesis and physicochemical properties of the graphene/ZrO_2 composite aerogels

Dongman Guo[1], Yun Lu[1,*], Yibo Zhao[2], Xuetong Zhang[1,3,*]

Received (in XXX, XXX) Xth XXXXXXXXX 20XX, Accepted Xth XXXXXXXXX 20XX

DOI: 10.1039/b000000x

Aerogel materials possess a wide variety of exceptional properties including quite low density, high specific surface area, high porosity, etc. Considered that both graphene aerogel and ZrO_2 aerogel have advantages and disadvantages respectively, the graphene/ZrO_2 composite aerogels are prepared by a facile step to enable them to have low thermal conductivity and to enhance the electronic interaction between ZrO_2 nanoparticles and graphene sheets. The chemical composition and crystalline structure of the resulting graphene/ZrO_2 composite aerogels, as well as the strong interaction between graphene sheets and ZrO_2 nanoparticles, have been disclosed by X-ray photoelectron spectroscopy (XPS), Raman spectroscopy and X-ray powder diffraction (XRD). The morphology and hierarchically porous attributes of the resulting graphene/ZrO_2 composite aerogels have been investigated by scanning electron microscopy (SEM), transmission electron microscopy (TEM) and nitrogen adsorption–desorption tests. The mechanical properties, electrical conductivity, electrochemical properties, thermal conductivity (as well as thermal stability) of the resulting graphene/ZrO_2 composite aerogels have also been revealed in this study.

1. Introduction

As a new kind of carbon material, graphene showed an excellent performance in energy storage, catalysis, polymer composites, electricity, etc., which is mainly attributed to its outstanding properties including high young's modulus, high fracture strength, large thermal conductivity, huge specific surface area, etc[1-3]. The graphene sheets decorated with metal oxide nanoparticles, such as ZnO, Fe_3O_4, TiO_2, MnO_2 and RuO_2, have attracted a great deal of scientific interest not only in basic scientific studies but also potential applications in fuel cells, solar cells, electronic devices, lithium ion batteries, gas sensors, etc.[4-8] Among the mental oxide nanoparticles, intensive attention should be paid to ZrO_2 with respect to its unique properties including excellent mechanical, electrical, thermal, optical, and stable photochemical properties. However, there have been a few reports about the graphene/ZrO_2 composites with application in lithium ion batteries, super-capacitors, detection of organic phosphorus agents so for. Shi et al. [9] have incorporated ZrO_2 nanoparticles into graphene sheets as a good candidate for the anode material of lithium-ion batteries. Das et al.[10] have synthesized graphene/ ZrO_2 composites by in-situ hydrothermal method. Du et al.[11] have mentioned preparation, characterization, and electrochemical properties of the graphene/ZrO_2 nano-composites and its application in enrichment and detection of methyl parathion. However none mentioned composites have been in the condensed state of the aerogel, and thus limited their applications in many fields due to the quite low specific surface area of these composites.

Aerogel materials possess a wide variety of exceptional properties including quite low density, high specific surface area, high porosity, etc. Due to above exceptional properties, aerogels are amongst the best thermal insulation materials and will likely be a promising insulation media in the future. To develop graphene composites in the form of the aerogel with low thermal conductivity, combining with the ZrO_2 is a good choice. The tetragonal and cubic ZrO_2 nanoparticles are used in insulating applications such as thermal barrier coatings. Zirconia aerogels are a kind of highly porous three-dimensional (3D) architectures with charming properties including low ratio of solid volume, and thus possess quite low heat transfer rate. A number of papers about ZrO_2 aerogel including designing catalyst supports [12-13] and electrodes in dye-sensitized solar cells [14] and solid oxide fuel cells (SOFCs) [15] were reported in the past few years. However, quite low electrical conductivity and extremely fragile mechanical properties have limited their applications in many fields. On the other hand, graphene aerogels with huge surface areas, large pore volumes and high conductivity have been successfully synthesized recently. Worsley M. A. et al.[16] have presented a unique method for producing ultra-low-density graphene aerogels with high electrical conductivities and large surface areas. An easy method to create graphene aerogels from aqueous gel precursors processed by supercritical CO_2 drying or by freeze drying has been reported in our previous work.[17] However inert nature of the graphene sheets has made the resulting graphene aerogels with inactive performances in many application fields. Considered that both graphene aerogel and ZrO_2 aerogel have advantages and disadvantages respectively, the graphene/ZrO_2

composite aerogels are prepared by a facile step to enable them to have low thermal conductivity and to enhance the electronic interaction between ZrO_2 nanoparticles and graphene sheets. By incorporation of ZrO_2 nanoparticles into graphene sheets, the aggregation problem of ZrO_2 nanoparticles could be minimized as well. Therefore, graphene sheets decorated with ZrO_2 nanoparticles combining with the outstanding properties of the aerogel materials might result in some particular properties according to the synergetic effect among them.

Different from all previously reported methods to prepare graphene/ZrO_2 composites, we have developed a facile route to synthesize graphene/ZrO_2 composite aerogels by using epichlorohydrin as a proton scavenger to initiate hydrolysis and polycondensation of dichlorooxozirconium $ZrOCl_2 \cdot 8H_2O$ in the graphene oxide/dimethylformamide (GO/DMF) solution to form the gel precursors, and then employing supercritical drying with CO_2 and carbonizing in argon in sequence to obtain the corresponding composite aerogels. The resulting graphene/ZrO_2 composite aerogels show quite low density (20-70 mg cm^{-3}), large specific surface area (380-490 m^2g^{-1}) and rather low thermal conductivity (0.0249-0.0259 $Wm^{-1}K^{-1}$). The experimental figures have also suggested the fact that the strong electronic interaction exists between ZrO_2 nanoparticles and graphene sheets.

2. Experimental

2.1 Chemical Reagents and Materials.

Graphite powder, $K_2S_2O_5$, P_2O_5, H_2SO_4, $KMnO_4$, H_2O_2, DMF, ethanol, etc. were purchased from Beijing Chemical Reagents Company without any further purification. GO used in this work has been synthesized according to the literature reported in our previous study.[17] High concentration GO/DMF solution has been prepared according to the procedure reported elsewhere.[18]

2.2 Preparation of the graphene/ZrO_2 composite aerogels.

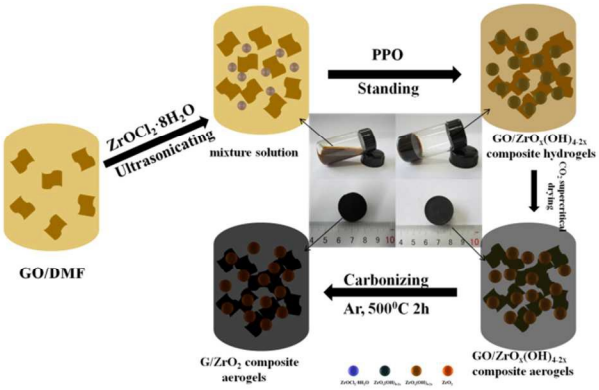

Figure 1. Schematic illustration for the synthesis of the graphene/ZrO_2 composite aerogels.

Synthesis of the graphene/ZrO_2 composite aerogels was illustrated in Figure1. Briefly, fixed amount of $ZrOCl_2 \cdot 8H_2O$ (0.115 g, 0.115 g and 0.043 g) was added respectively to GO/DMF solution (6 mg/ml, 12 mg/ml and 12 mg/ml) to form uniform mixture, then epichlorohydrin (PPO) was added to above mixture with stirring for a short while and then standing still over some time to form the gel. The resulting graphene/ZrO_2 composite aerogels would be obtained as long as above composite gels after 3-day aging were processed with solvent-exchange with ethanol, supercritical fluid drying with CO_2 and then carbonization under 500 ^{0}C for 2h in Ar atmosphere in sequence. Need to point out that, lower carbonization temperature could not fully convert precursors into the final products, and higher carbonization temperature could reduce specific surface area of the resulting composite aerogels.

2.3 Characterization.

The structures and compositions of the as-prepared products were characterized by X-ray powder diffraction (XRD) using a Rigaku Dmax 2200 X-ray diffractometer with Cu K_α radiation (λ= 1.5416 Å). Raman spectra were recorded on a Lab RAM HR800 (Horiba Jobin Yvon) confocal Raman spectrometer with an excitation laser wavelength of 632.8 nm. All samples were deposited on silicon wafers without using any solvent. The morphology of the composite was observed with a scanning electron microscope (SEM, Hitachi S-4800). Transmission electron microscopy (TEM) and high-resolution TEM (HRTEM) investigations were carried out by a FEI Teanai 20 microscope. The as-prepared samples were dispersed in deionized water and dropped onto a carbon film supported on a copper grid for the drying process in air. The X-ray photoelectron spectroscopic (XPS) study was performed using the Kratos Axis-ULTRA XPS analyzer. The X-ray source used was amonochromatic Al K_α line ($h\upsilon$ = 1486.71 eV) powered with 10 mA and 15 kV. Thermogravimetric analysis (TGA) was performed in air using a Pyris Diamond TG/DTA (PerkinElemer Inc., U.S.A). The samples were heated from room temperature to 900 °C at 10 °C/min. Specific surface areas were measured at 77 K by Brunauer–Emmett–Teller (BET) nitrogen adsorption–desorption (Shimadzu, Microm eritics ASAP 2010 Instrument), and pore size distributions were calculated from the desorption branch of the N_2 adsorption isotherm using the Barrett–Joyner– Halenda (BJH) formula. Thermal conductivity of the composite aerogels and graphene aerogel were investigated by hot wire technique with the Thermal Conductivity Measuring Instrument (TC3010L). The conductivity of as-prepared composite aerogels and graphene aerogel were characterized by *I–V* curves (Electrochemical workstation). The mechanical properties of composite aerogels were measured by Instron 6022 instrument, the stroke was 40% of the sample length, and the velocity was 30% of the sample length/min. The ZrO_2/graphene composite aerogels were packed into nickel foam in a sandwich-type as the test electrode, an Ag/AgCl electrode was used as the reference electrode, and 1 M KOH were used as the electrolyte, respectively. The electrochemical performance was investigated by using the Solartron 1280B electrochemical workstation to carry out the cyclic voltammetry (CV) and by using the Arbin cell tester (CT2001A) to carry out galvanostatic charge/discharge tests.

3. Results and discussion

X-ray diffraction (XRD) is employed to determine the crystalline phase of sample and the XRD patterns of all samples are shown in Figure 2. After calcinations at 500 ^{0}C, the graphene/ZrO_2 composite aerogels exhibited a single tetragonal

ZrO_2 (t-ZrO_2). Five peaks at 2θ=30.1, 35.1, 50.2, 59.2 and 74.6^0 are obvious in the ZrO_2 aerogel and composite aerogels, consistent with (101), (110), (200), (211) and (220) crystalline plane of the t-ZrO_2（JCPDS NO. 88-1007). A strong diffraction peek 2θ=24^0, which is ascribed to the (002) diffraction of graphene [19-20], indicating that the GO was completely reduced to graphene.[21] There are no obvious peaks corresponding to graphene observed in the graphene/ZrO_2 composite aerogel pattern, which might be attributed to that the graphene sheets have been evenly dispersed in the composite aerogel owing to the ability that ZrO_2 nanoparticles can evenly spread among graphene layers. It also indicates that the growth of the crystalline phase of ZrO_2 nanoparticles is not influenced by the existence of graphene sheets.

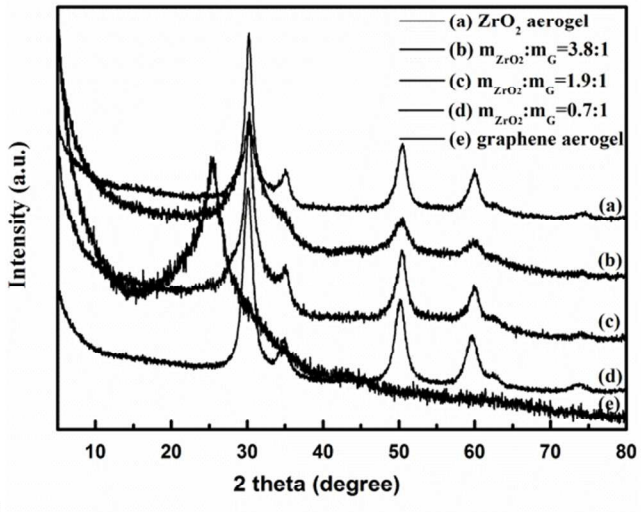

Figure 2. XRD patterns of ZrO_2 aerogel (a), graphene/ZrO_2 composite aerogels with mass ratios of ZrO_2 to graphene=3.8:1 (b), 1.9:1 (c), 0.7:1 (d) and graphene powder (e).

Raman spectroscopy is a powerful tool to characterize carbonaceous materials, especially the sp^2 and sp^3 hybridized carbon atoms involved in GO and graphene. The graphene powder, graphene/ZrO_2 composite aerogels were investigated by Raman spectroscopy and the results were displayed in Figure 3a. Both D and G band can be reserved in the Raman spectra of above all samples. But the G bands of the graphene/ZrO_2 composite aerogels occur to 8 cm^{-1} blue shift in comparison with that of the graphene powder. The results indicate that the graphene/ZrO_2 composite aerogels contain graphene sheets really and the existence of ZrO_2 in the graphene/ZrO_2 composite aerogels can influence the graphene sheets (the existence of the electronic interaction between ZrO_2 and graphene sheets [22]). The D band is an indication of the defects and disorder vibrations of sp^3 carbon atoms, and the G band is related to the vibration of sp^2 carbon atoms in a graphitic 2D hexagonal lattice.[23] Therefore, the intensity of the D and G bond (I_D/I_G) gives the clue to the ordered or disordered crystal structures of graphene sheets.[24-26] The intensity ratios of I_D/I_G of the composite aerogels after heat treatment at 500^{0}C increase from 0.96 to 1.17 as the mass ratios of ZrO_2 to graphene decrease from 3.8:1 to 0.7:1, are similar to the intensity of graphene aerogel (I_D/I_G=1.12), indicating the reduction of graphene oxide to graphene after the heat treatment.

The as-prepared graphene/ZrO_2 composite aerogels were analysed by TGA. As is shown in Figure 3b, the composite aerogels have exhibited mainly four stages of weight loss with the temperature range of 25–900^{0}C. The first stage of weight loss (ca.2%) up to 100–110^{0}C can be attributed to the loss of adsorbed water molecules. The second stage from 110 to 300^{0}C is ca.3%, which is attributed to the removal of chemisorbed water and organics in the mesopores of the composite aerogels, as well as organic functional groups in the graphene sheets located in the composite aerogels. The third weight loss (ca.3%) occurs at 430-600^{0}C, which is associated with the loss of the thermal oxidative decomposition of the graphene sheets and the condensation of the ZrO_2 nanoparticle precursors [27]. The last stage of weight loss is ca.7%, which is attributed to the loss of further thermal oxidative decomposition of the graphene sheets. From the above results, it suggested that the graphene/ZrO_2 composite aerogels show good thermal stability.[18]

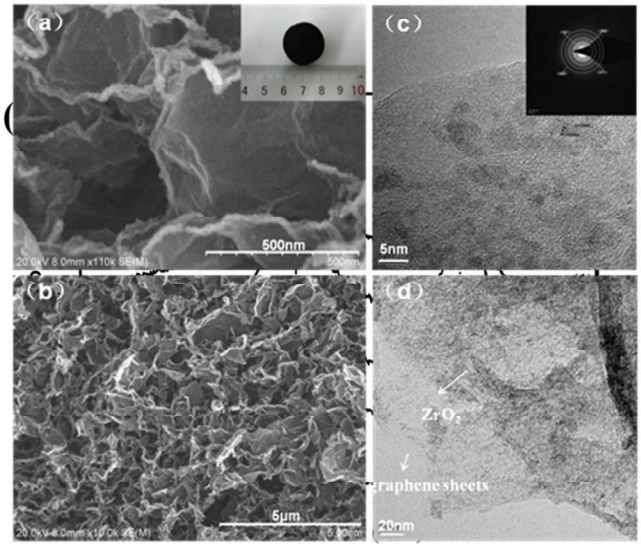

Figure 5. SEM images of graphene/ZrO_2 composite aerogel with different magnification (a, b). Inset in (a) is a digital photo of the composite aerogel. TEM images of graphene/ZrO_2 composite aerogel with different magnification. Inset in (c) is the selected area electron diffraction (SAED) pattern.

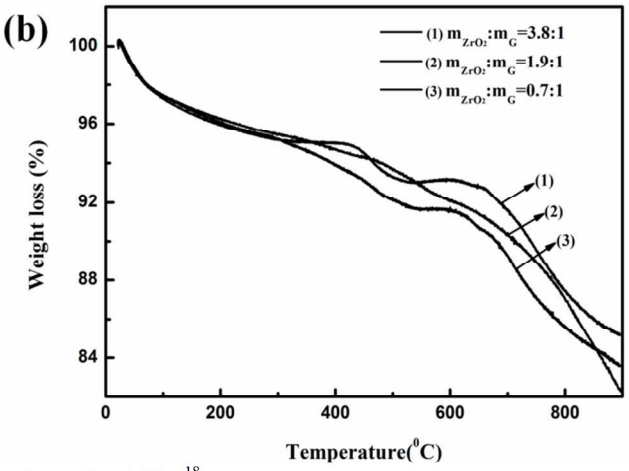

Figure 3. (a)Raman spectra of graphene aerogel (1) and graphene/ZrO_2 composite aerogels with mass ratios of ZrO_2 to graphene =3.8:1 (2), 1.9:1 (3), 0.7:1 (4); (b) TGA curves of the resulting graphene/ZrO_2 composite aerogels with mass ratios of ZrO_2 to graphene =3.8:1 (1), 1.9:1 (2), 0.7:1 (3).

The chemical structure of the GO powder and graphene/ZrO_2 composite aerogels were studied by X-ray photoelectron

Figure4. XPS survey profiles of the GO powder and graphene/ZrO_2 composite aerogel (a), Zr 3d XPS pattern of the graphene/ZrO_2 composite aerogel (b), C 1s of XPS spectra of the GO powder (c) and graphene/ZrO_2 composite aerogel (d).

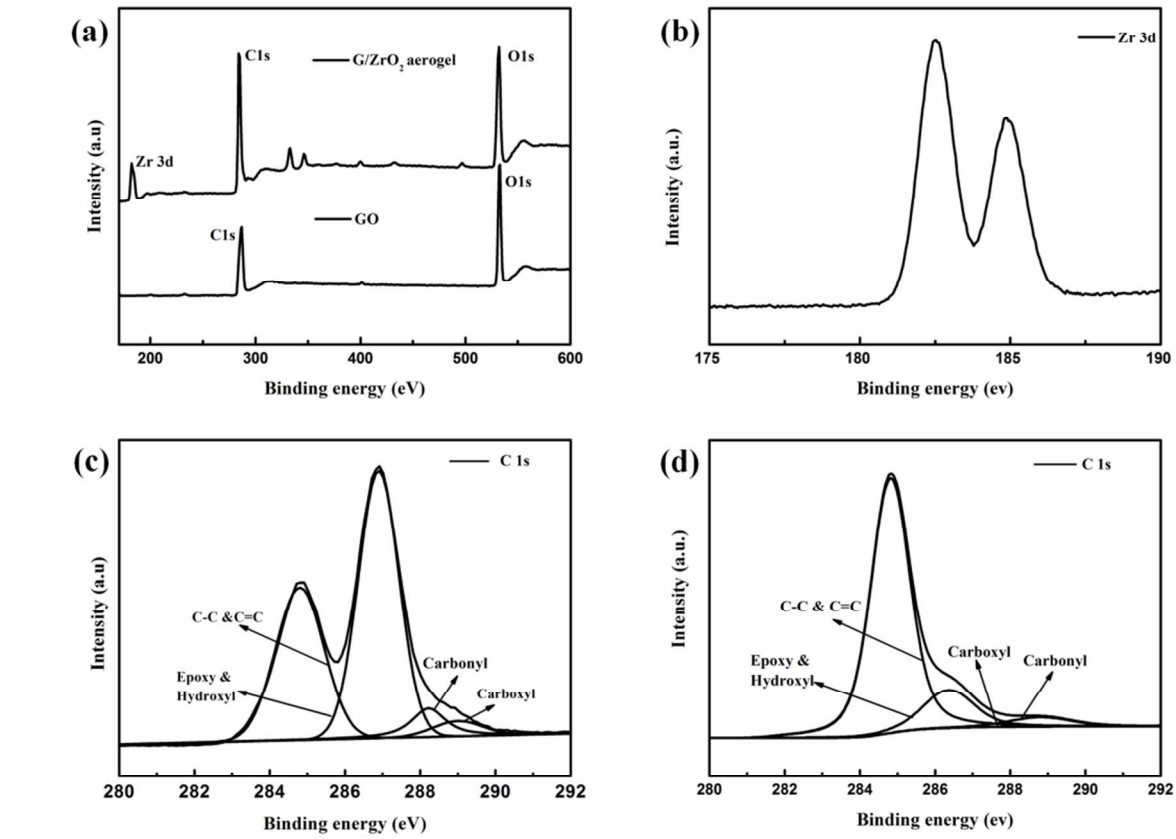

graphene/ZrO_2 composite aerogel and GO powder, which reveal the presence of carbon and oxygen elements. In comparison with GO, the Zr peak is only observed from graphene/ZrO_2 composite aerogel. From Figure 4(b), the Zr 3d peaks are obviously observed in the graphene/ZrO_2 composite aerogel. The Zr $3d_{5/2}$ and Zr $3d_{3/2}$ peaks have binding energies of 182.5 and 184.9 eV, respectively, which represent the fully oxidized zirconium ions in its Zr^{4+} state.[28-29] The C 1s spectrum of the GO powder contains four functional groups: the non-oxygenated ring C (284.7 eV), C–OH species (286.7 eV), C=O species (288.1eV) and C=O–OH (289.1 eV) in Figure 4(c).[30] Although the C 1s spectrum of graphene/ZrO_2 composite aerogel shows the same oxygen functionalities as GO powder, the absorbance peak intensities of the composite aerogel at 286.7 eV (C–OH), 288.1eV (C=O), 289.1 eV (C=O–OH) were sharply decreased, and the intensity of the non-oxygenated ring C (284.7 eV) peak increases simultaneously in Figure 4(d). The results describe the fact that most of the oxygenated functional groups are successfully removed after high temperature treatment, suggesting the reduction of graphene oxide to graphene.

The morphology and structural feature of the as-prepared graphene/ZrO_2 composite aerogel have been elucidated by scanning electron microscope (SEM) and transmission electron microscope (TEM). Figure 5a presents the representative SEM image of the composite aerogel, revealing ruffled morphology consisting of thin wrinkled structure and nanoparticles. It also can been seen that small ZrO_2 nanoparticles are homogeneously distributed on graphene sheets and between the layers of them.

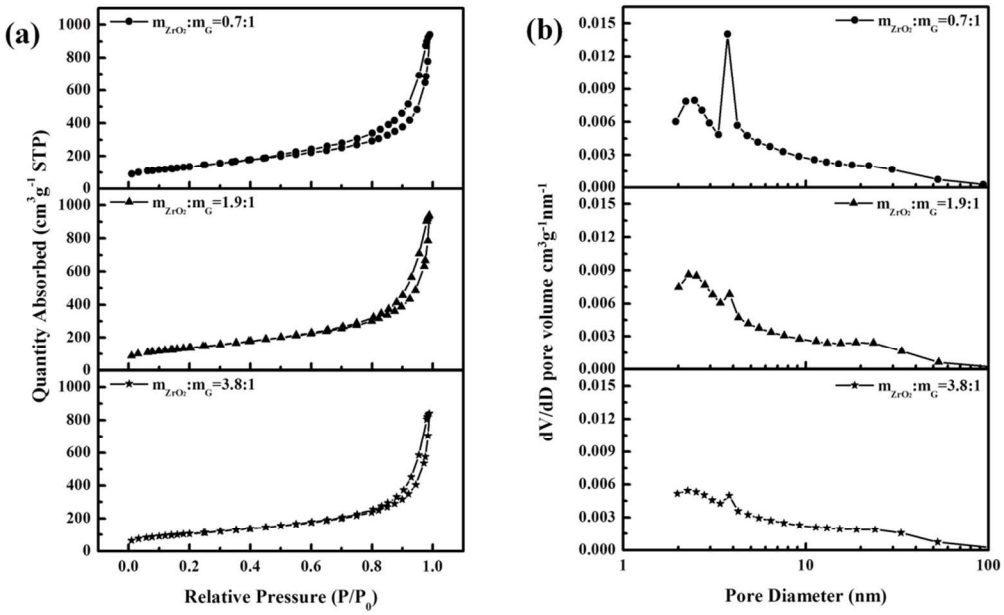

Figure 6. N_2 adsorption-desorption isotherms (a) and pore-size distribution curves (b) of the graphene/ZrO_2 composite aerogels with different mass ratios of ZrO_2 to graphene.

Due to the presence of graphene sheets, the monolithic graphene/ZrO_2 composite aerogel (inset in Figure 5a) were easily obtained in comparison with the monolithic ZrO_2 aerogel (the latter is too fragile), indicating that the graphene sheets can enhance the mechanical strength of the ZrO_2 aerogel (More details see Supporting Information Figure SI1 and Table SI1). It can be seen from Figure 5b that a lot of large open pores are uniformly distributed within the graphene/ZrO_2 composite aerogel. A HRTEM image of graphene/ZrO_2 composite aerogel is shown in Figure 5c, showing the average particle size of the ZrO_2 is less than 10 nm and a lattice spacing of 0.32 nm, corresponding to the d-spacing of (101) crystal plane of t-ZrO_2. The insets in Figure 5c and Figure SI2 are the selected area electron diffraction (SAED) patterns of the composite aerogel and pure ZrO_2 aerogel respectively, indicating that the results are consisted with those revealed by XRD. Compared with the composite aerogels, ZrO_2 nanoparticles in the pure ZrO_2 aerogel have aggregated easily, as shown in Figure S2b-d. The results suggest that the large surface area of graphene sheets provide a good support for ZrO_2 nanoparticles and prevent their aggregation. Figure 5d is the HRTEM image, also showing that graphene sheets are uniformly decorated by ZrO_2 nanoparticles. Although the sample processed with ultrasonic treatment, the ZrO_2 nanoparticles disperse well on the graphene sheets, which indicates the existence of strong interaction between graphene sheets and ZrO_2 nanoparticles.

The porous property of the graphene/ZrO_2 composite aerogels is further confirmed by the nitrogen sorption investigations. N_2 adsorption-desorption isotherms and pore-size distribution curves of the graphene/ZrO_2 composite aerogels with different mass ratios of ZrO_2 to graphene were presented in Figure 6. All the adsorption-desorption curves exhibit type- IV isotherm with a H_3 hysteresis loop, suggesting a characteristic of open wedge-shaped mesoporous structure.[31] The BET surface areas of the graphene/ZrO_2 composite aerogels was in the range 388-490 m^2g^{-1}, which was much higher than that of the bare ZrO_2 aerogel.[32-33] The lower mass ratio of ZrO_2 to graphene (e.g., 0.7) would not effectively reduce the aggregation of the graphene sheets, while the higher mass ratio (e.g., 3.8) would not effectively reduce the aggregation of the ZrO_2 nanoparticles, and thus the highest BET surface area would be obtained for the composite aerogel with the mass ratio of ZrO_2 to graphene at 1.9. The high surface area is an essential factor for the low thermal conductivity of graphene/ZrO_2 composite aerogels. The vast majority of pores (shown as in Figure 6b) in the range of 2-100 nm, which indicates the presence of relatively well-defined mesoporous. The total pore volume is 1.30-1.45 cm^3g^{-1} for composite aerogels. The nitrogen sorption data of the graphene/ZrO_2 composite aerogels

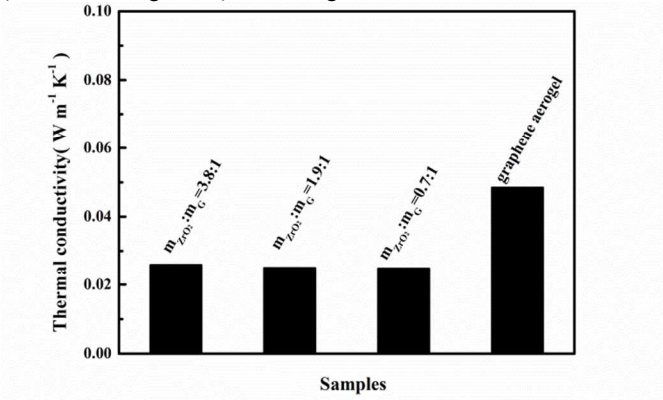

with quite low apparent densities (20-70 mg cm^{-3}) were shown in Table SI2.

Figure 7. Thermal conductivities of the graphene aerogel and graphene/ZrO_2 composite aerogels with different mass ratios of ZrO_2 to graphene.

In order to investigate the heat conduction properties of the graphene/ZrO_2 composite aerogels, thermal conductivity experiments were conducted at the room temperature and the results are listed in Table SI3. The ZrO_2 nanoparticles are used in insulating applications such as thermal barrier coatings.[34] Figure7 illustrates thermal conductivity of the graphene aerogel and graphene/ZrO_2 composite aerogels with different mass ratios of ZrO_2 to graphene. The results show that the graphene/ZrO_2 composite aerogels have a lower thermal conductivity than that of the graphene aerogel. At room temperature, the thermal conductivity of graphene/ZrO_2 composite aerogels with different mass ratios of ZrO_2 to graphene is close to each other. But the thermal conductivity of the graphene aerogel with higher specific surface area and porosity is about two times larger than those of the graphene/ZrO_2 composite aerogels. It has been pointed out that a number of factors including density, porosity, specific surface area, etc., would effectively have an influence on the thermal conductivity of porous materials. It has been proved that microstructural parameters such as grain size or porosity of nanoparticles have heavy effects on the thermal conductivity of materials. In particular, smaller grain size resulting in a higher number of grain boundaries in the heat path can add additional thermal resistance to the polycrystalline solid phase. The presence of small ZrO_2 nanoparticles effectively increases the grain boundaries in the graphene/ZrO_2 composite aerogels in our present work.

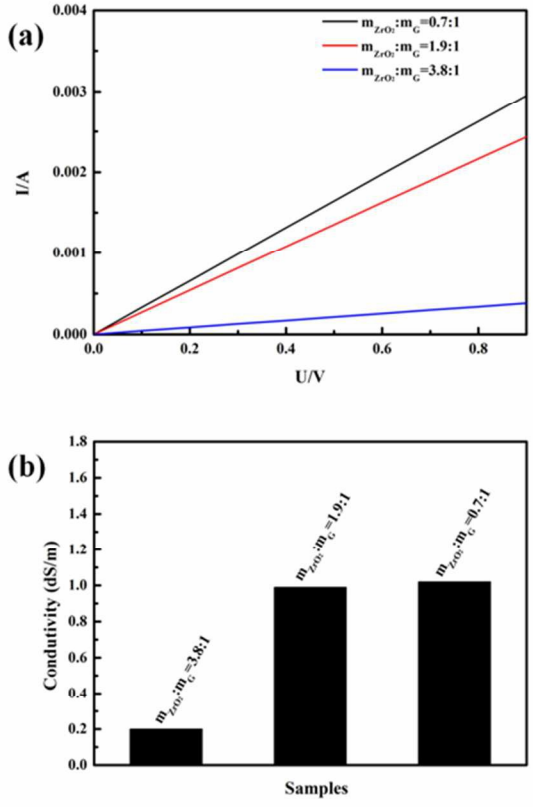

Figure 8. *I–V* curves (a) and conductivity histograms (b) of the graphene/ZrO_2 composite aerogels with different mass ratios of ZrO_2 to graphene.

At the room temperature, the pure ZrO_2 nanoparticles have an extremely high resistance, namely, ZrO_2 nanoparticles are insulation materials. The presence of reduced graphene oxide in the graphene/ZrO_2 composite aerogels promotes electronic interaction with ZrO_2, which enhancing the conductivity of the composite aerogels. The linear cycle voltammetry of graphene/ZrO_2 composite aerogels with different mass ratios of ZrO_2 to graphene and graphen aerogel have been represented in Figure 8a and Figure SI3. In comparison with graphene aerogel, the conductivity of composite aerogels obviously decreased. Figure 8b and Figure SI3 have shown the conductivity of the graphene/ZrO_2 composite aerogels with different mass ratios of ZrO_2 to graphene and the conductivity of the graphene aerogel, respectively. In fact, the experimental observation of the graphene conductivity decreases after ZrO_2 decoration.

To further study the electrochemical energy storage of the composite aerogels, the electrochemical investigations have been conducted, as shown in Figure SI4. For the composite aerogel with the mass ratio of ZrO_2 to graphene at 0.7, even when the scan rate increases to 100 mVs^{-1}, the cyclic voltammograms (Figure SI4a) of composite aerogel basically remain rectangle shapes with some deviation at lower potential, implying a quick charge propagation capability of both double layer capacitance and pseudo-capacitance. Meanwhile, the rate performances of the composite aerogels were also evaluated by galvanostatic charge/discharge under an enhanced current density (Figure SI4b). The capacitance of composite aerogel decreases slowly with an increase of the current density, indicating that the composite aerogel show good rate capability. When the current density is 0.5 Ag^{-1}, the specific capacitance of the composite aerogel is 117 Fg^{-1}, however when the current density increases as high as 10 Ag^{-1}, the specific capacitance of the composite aerogel still remains 52 Fg^{-1}. Furthermore, the electrochemical impedance spectroscopy (EIS) plots (Figure SI4c) of the cell based on the composite aerogel shows the typical electric double layer capacitive behaviour. The intercept of the composite aerogel is 0.471 Ω cm^2, indicating that the resistance of the cell based on the composite aerogel is not very high. The cycle performance (Figure SI4d) of the capacitor based on of the graphene/ZrO_2 composite aerogel is relatively stable. However, for the composite aerogels with the higher mass ratios of ZrO_2 to graphene, the electrochemical energy storage performances are not as that of the composite aerogel with the mass ratio of ZrO_2 to graphene at 0.7, as shown in Figure SI5.

4. Conclusions

A low-cost and simple method was reported to synthesize graphene/ZrO_2 composite aerogels, in which the graphene sheets were decorated with ZrO_2 nanoparticles. The resulting composite aerogels have possessed a mesoporous structure (pore diameter

lies at ca.13 nm) with low density (20-70 mg cm^{-3}) and large specific surface area (380-490 m^2g^{-1}). On the other hand, physicochemical properties of the graphene/ZrO_2 composite aerogels were fully conducted by many experiments, suggesting superior thermal stability, low thermal conductivity at room temperature and appropriate electrochemical performance.

Acknowledgement

This work was financially supported by the National Natural Science Foundation of China (21373024), the Innovation Program of the Beijing Institute of Technology and the 100 Talents Program of the Chinese Academy of Sciences.

Notes and Reference

[1] *School of Materials Science and Engineering, Beijing Institute of Technology, Beijing 100081, P. R. China. E-mail: luyun@bit.edu.cn; zhangxtchina@yahoo.com*
[2] *Aerospace Research Institute of Materials and Processing Technology, Beijing, 100076, P. R. China*
[3] *Suzhou Institute of Nano-Tech & Nano-Bionics, Chinese Academy of Sciences, Suzhou 215123, P. R. China*

† Electronic Supplementary Information (ESI) available: [More SEM and TEM images, Nitrogen sorption data and thermal conductivity data, etc.]. See DOI: 10.1039/b000000x/

1.K. S. Novoselov, A. K. Geim, S. V. Morozov, D. Jiang, Y. Zhang, S. V. Dubonos, I. V. Grigorieva and A. A. Firsov, *Science*, 2004, **306**, 666-669.
2. A. K. Geim, K. S. Novoselov, *Nat. Mater.* 2007, **6**, 183−191.
3. A. K. Geim. *Science*, 2009, **324**, 1530−1534.
4. Z. Y. Yin, S. X. Wu, X. Z. Zhou, X. Huang, Q. C. Zhang, F. Boey and H. Zhang, *Small*, 2010, **6**, 307.
5. X. Y. Yang, X. Y. Zhang, Y. F. Ma, Y. Huang, Y. S. Wang and Y. S. Chen, *J. Mater. Chem.*, 2009, **19**, 2710.
6. T. N. Lambert, C. A. Chavez, B. Hernandez-Sanchez, P. Lu, N. S. Bell, A. Ambrosini, T. Friedman, T. J. Boyle, D. R. Wheeler and D. L. Huber, *J. Phys. Chem. C*, 2009, **113**, 19812.
7. S. Chen, J. W. Zhu, X. D. Wu, Q. F. Han and X. Wang, *ACS Nano*, 2010, **4**, 2822.
8. Z. S. Wu, D. W. Wang, W. C. Ren, J. P. Zhao, G. M. Zhou, F. Li and H. M. Cheng, *Adv. Funct. Mater.*, 2010, **20**, 3595.
9. H. Xu, S. Yuan, Z. Wang, Y. Zhao, J. Fang and L. Shi, *RSC Advances*, 2014, **4**, 8472.
10. S. Giri, D. Ghosh and C. K. Das, *Advanced Functional Materials*, 2014, **24**, 1312-1324.
11. D. Du, J. Liu, X. Zhang, X. Cui and Y. Lin, *Journal of Materials Chemistry*, 2011, **21**, 8032.
12. S. Cimino, R. Pirone, L. Lisi, *Appl. Catal., B* 2002, **35**, 243.
13. A. Bahamonde, S. Campuzano, M. Yates, P. Salerno, S. Mendioroz, *Appl. Catal., B* 2003, **44**, 333.
14 .Y. Diamant, S. Chappel, S. G. Chen, O. Melamed, A. Zaban, *Coord. Chem. Rev.* 2004, **248**, 1271.
15. K. Yamahara, T. Z. Sholklapper, C. P. Jacobson, S. J. Visco, L. C. de Jonghe, *Solid State Ionics* 2005, **176**, 1359.
16. M. A. Worsley, P. J. Pauzauskie, T. Y. Olson, J. Biener, J. H. Satcher, and T. F. Baumann, *J. Am. Chem. Soc.* 2010, **132**, 14067–14069.
17. X. Zhang, Z. Sui, B. Xu, S. Yue, Y. Luo, W. Zhan and B. Liu, *Journal of Materials Chemistry* 2011, **21**, 6494.
18. L. Chen, B. Wei, X. Zhang and C. Li, *Small* 2013, **9**, 2331-2340.
19. J. K. Lee , K. B. Smith , C. M. Hayner , H. H. Kung , *Chem. Commun.* 2010 , **46** , 2025 .
20. J. Z. Wang , C. Zhong , S. L. Chou , H. K. Liu , *Electrochem. Commun.* 2010 , **12** , 1467 .
21. M. Zhou, Y. Zhai and S. Dong, *Anal. Chem.*, 2009, **81**, 5603.
22. F. H. Li, J. F. Song, H. F. Yang, S. Y. Gan, Q. X. Zhang, D. X. Han, A. Ivaska, L. Niu, *Nanotechnology* 2009, **20**, 455602.
23. C. H. Xu, B. H. Xu, Y. Gu, Z. G. Xiong, J. Sun and X. S. Zhao, *Energy Environ. Sci.* 2013, **6**, 1388–1414.
24. H. L. Wang, J. T. Robinson, X. L. Li and H. J. Dai, *J. Am. Chem. Soc.* 2009, **131**, 9910;
25. A. B. Bourlinos, D. Gournis, D. Petridis, T. Szabo, A. Szeri and I. Dekany, *Langmuir*, 2003, **19**, 6050;
26.W. F. Zhao, M. Fang, F. R. Wu, H. Wu, L. W. Wang and G. H. Chen, *J. Mater. Chem.* 2010, **20**, 5817.
27. L. L. Hench, J. K. West, *Chem. Rev.* 1990, **90**, 33-72.
28. J. S. Xue and J. R. Dahn, *J. Electrochem. Soc.* 1995, **142**, 3668–3677.
29. T. L. Barr, *J. Phys. Chem.* 1978, **82**, 1801–1810.
30. J.Hu, H. Li and X.Huang, *Solid State Ionics* 2007, **178**, 265–271.
31. S. B. Yang, X. L. Feng, K. Mullen , *Adv. Mater.* 2011, **23**, 3575 .
32. B. Tyagi, K. Sidhpuria, B. Shaik, and R. V. Jasra, *Ind. Eng. Chem. Res.* 2006, **45**, 8643-8650
33. R. Sui, A.S. Rizkalla and P. A. Charpentier, *Langmuir* 2006, **22**, 4390-4396
34. F. Pennec, A. Alzina, B. N. Ali, N. Tessier-Doyen, D.S. Smith, *Computational Materials Science* 2013,**67**, 207 − 215.